Long-Lifetime Optical Trapping of a $^{40}Ca^{+}$ Ion

Zheng Chen(陈正)[1,2,3†], Miao Wang(王淼)[1,2†], Baolin Zhang(张宝林)[1,2], Huaqing Zhang(张华青)[1,2], Zixiao Ma(马子晓)[1,2,3], Ruming Hu(胡如明)[1,2,3], Yao Huang(黄垚)[1,2*], Kelin Gao(高克林)[1,2], and Hua Guan(管桦)[1,2,4]

[1]*State Key Laboratory of Magnetic Resonance and Atomic and Molecular Physics, Innovation Academy for Precision Measurement Science and Technology, Chinese Academy of Sciences, Wuhan 430071, China*
[2]*Key Laboratory of Atomic Frequency Standards, Innovation Academy for Precision Measurement Science and Technology, Chinese Academy of Sciences, Wuhan 430071, China*
[3]*University of Chinese Academy of Sciences, Beijing 100049, China*
[4]*Wuhan Institute of Quantum Technology, Wuhan 430206, China*

(Received 11 August 2024; accepted manuscript online 27 September 2024)

We have experimentally achieved the all-optical trapping of a $^{40}Ca^{+}$ ion. An optical dipole trap was established using a high-power, far-detuned, tightly focused laser with a wavelength of 532 nm. The single $^{40}Ca^{+}$ ion was trapped without any RF fields and demonstrated a long lifetime of over 3 s. In this experiment, we implemented several measures to improve the optical trapping probability, including focusing the dipole beam waist near the diffraction limit, precisely compensating for stray electric fields, and mitigating electron shelving in metastable states. The optical trapping of a $^{40}Ca^{+}$ ion eliminates the influence of micromotion induced by RF fields, potentially paving the way for development of all-optical trapping ion optical clocks.

DOI: 10.1088/0256-307X/41/11/113701

Isolating ions and atoms from the environment and trapping them stably for long periods is of great significance in the field of precision measurement physics,[1–3] especially for experiments at the quantum level.[4,5] For several decades, this has been achieved by trapping ions with RF fields[6] and neutral particles with optical fields,[7] respectively. These techniques have made remarkable progress in recent years.[8–10] However, for RF field-trapped ions, the RF-induced micromotion imposes a significant constraint on the accuracy of precision measurements.[11,12] State-of-the-art ion optical clocks have now reached an accuracy at the level of 10^{-18} [13–17] or higher,[1–3] which is mainly limited by the influence of micromotion.[1,14,18] Additionally, micromotion also restricts experiments in ultracold chemistry,[19,20] quantum simulation,[21] and quantum computation[22] at present.

In order to further improve the development of ion optical clocks, a generic solution for the elimination of micromotion in trapped ions is urgently needed. In 2010, Schaetz's group demonstrated the optical trapping of a single ion without any RF fields.[23] In that work, a $^{24}Mg^{+}$ ion was trapped in an optical dipole trap superimposed with a static electric potential. Due to the absence of RF fields, the influence caused by micromotion was naturally eliminated. Building on this foundation, Schaetz's group demonstrated the optical trapping of a single $^{138}Ba^{+}$ ion with significant long lifetimes[24,25] and coulomb crystals in an optical lattice.[26,27] Additionally, they observed Feshbach resonances between an optically trapped ion and ultracold atoms in recent years,[28,29] making a significant contribution to the field of ultracold chemistry. Aside from $^{24}Mg^{+}$ and $^{138}Ba^{+}$, ion optical clocks are also based on the trapping of $^{27}Al^{+}$ (Ref. [1]), $^{40}Ca^{+}$ (Ref. [16]), $^{88}Sr^{+}$ (Ref. [30]), $^{171}Yb^{+}$ (Ref. [31]), $^{176}Lu^{+}$ (Ref. [2]), $^{199}Hg^{+}$ (Ref. [32]), and other ions. However, no further works on the optical trapping of other ions have been demonstrated for ion optical clocks to date.

In this Letter, we demonstrated the optical trapping of a $^{40}Ca^{+}$ ion, intended for use in $^{40}Ca^{+}$ ion optical clocks. We established a new experimental platform for optically trapping and successfully achieved the longest optical trapping lifetime of over 3 s for a single Ca^{+} ion. By utilizing the all-optical trapping technique, the systematic frequency shifts of $^{40}Ca^{+}$ ion optical clocks caused by micromotion will be eliminated, as the RF field is switched off. This work could pave the way for the development of all-optical trapping ion optical clocks.

Experiment. The experimental scheme for optical trapping of a single $^{40}Ca^{+}$ ion, as shown in Fig. 1, involves the following steps: Firstly, the ion is trapped by RF fields and cooled to the Doppler limit in a Paul trap. Then, an optical dipole trap (ODT) is established along the Paul trap's axial direction (z-axis), with its beam waist focused on the ion's position, and effectively replaced the RF fields to trap the ion for a period of time. Finally, we transfer the ion back to RF fields and monitor the fluorescence light

†These authors contributed equally to this work.
*Corresponding author. Email: yaohuang@apm.ac.cn
© 2024 Chinese Physical Society and IOP Publishing Ltd

scattered off the ion from the Doppler cooling laser using a charge-coupled device (CCD) camera. This reveals with near unity efficiency whether the ion was lost during the experimental sequence. Trapping according to the above sequence is repeated until the ion is lost.

In our work, a segmented linear Paul trap with a minimum 3 mm distance from its center to the RF electrodes was selected to generate the RF field with a trapping frequency $\Omega_{\rm RF} \approx 2\pi \times 9.33$ MHz. To ensure successful optical trapping of a $^{40}Ca^{+}$ ion, dc electric fields are maintained throughout the entire experimental sequence to provide sufficient axial confinement and prevent the ion from escaping along the propagation direction of the dipole laser. Additionally, two prerequisites for successful optical trapping are ensured:[33] (1) The trapping potential of the ODT should be higher than the ion's kinetic energy. (2) The residual force of stray electric fields at the ion's position should be at least one order of magnitude smaller than the maximal dipole force of the dipole trap.

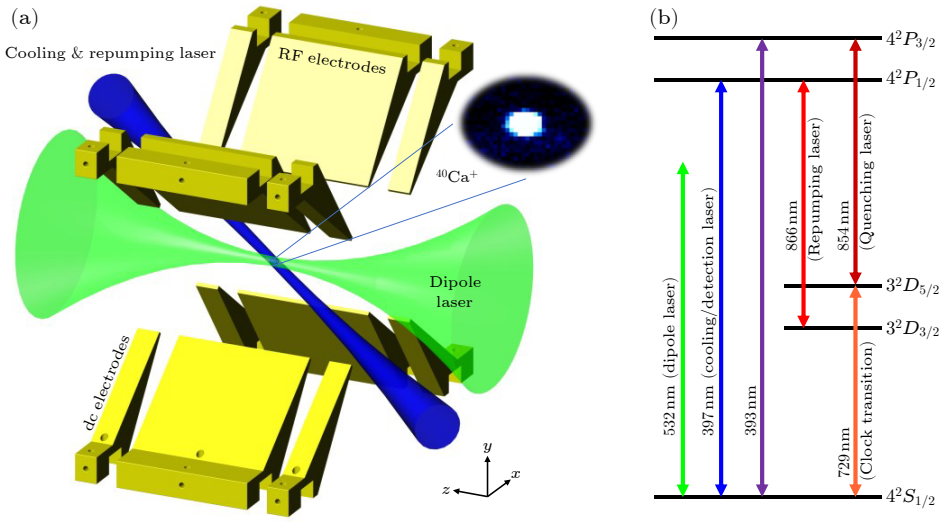

Fig. 1. (a) Schematic of the experimental setup (not to scale). Inset: the imaging of a single $^{40}Ca^{+}$ ion observed by the CCD camera. (b) Relevant energy levels and optical transitions of a $^{40}Ca^{+}$ ion.

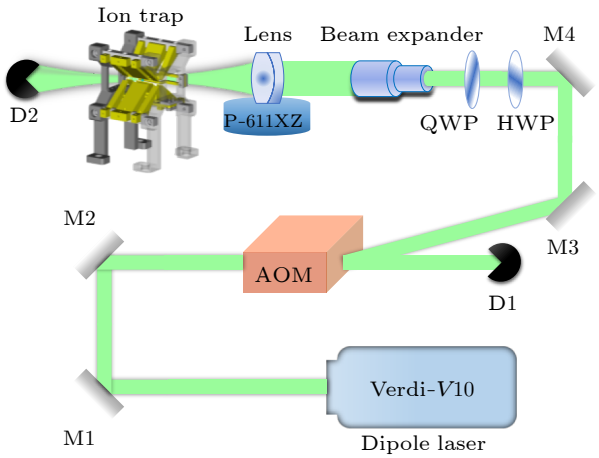

Fig. 2. Schematic diagram of the dipole laser beam path. M: mirror; D: beam dump; HWP: half-wave plate; QWP: quarter-wave plate; AOM: acousto-optic modulator.

Optical Dipole Trap. Optical dipole traps (ODTs) rely on the mechanism that the induced atomic dipole moment interacts with the intensity gradient of a far-detuned light field, known as the dipole force. The potential wells of ODTs are utilized for trapping atoms due to the conservative nature of the dipole force.[33] For the optically trapping of a $^{40}Ca^{+}$ ion, using a dipole laser near the dipole resonant transition $4S \leftrightarrow 4P$ [corresponding to lasers of 397 nm and 393 nm, as depicted in Fig. 1(b)] would lead to a high heating rate caused by photon recoils out of the ODT, thereby limiting the trapping lifetime.[23,26] Therefore, we opt for a high-power, far-detuned laser with a wavelength of 532 nm to establish the ODT, ensuring a sufficiently high trapping potential and low photon recoiling rate.

The dipole laser is generated from a diode-pumped solid-state (DPSS) laser system (Coherent, Verdi-V10) with a frequency of $\omega = 2\pi c/(532\,\text{nm})$ and a maximal output power of $P_{\rm max} = 10$ W. Figure 2 shows a schematic beam path of the dipole laser. Firstly, the dipole laser is split with an acousto-optic modulator (AOM, custom-made specifically for optical switching), achieving up to 85% diffraction efficiency to switch the laser within timescales of $t < 500$ ns and to adjust the power. Then, while the zeroth order light is collected by a beam dump, the first order light, after passing through a set of half-wave plate (HWP) and quarter-wave plate (QWP) to ensure a polarization with maximum trapping potential depth, is enlarged with a 1 : 10 beam expander (JENOPTIK, Beam-Expander var. 2x-10x 532 nm) to a diameter of $D \approx 35$ mm. Finally, the enlarged beam is focused with a lens objective (Qioptiq, LINOS Focus-Ronar) featuring a focal lens of $f = 77$ mm to establish an ODT at the trap center, resulting in an expected minimum beam waist radius at the position of the ion:

$$w_{\rm min} = \frac{f\lambda}{D} \approx 1.17\,\mu\text{m}, \tag{1}$$

according to the diffraction limit. To ensure a smooth

spatial intensity Gaussian profile of the ODT at the ion's position, the optical axis of all the optical elements has to be carefully aligned with the laser beam propagation axis.

After passing through all the optical elements, the dipole laser reaches a power of up to $P_{\text{enter}} \leq 5.38\,\text{W}$ entering the chamber, which could be tuned with the AOM. According to the diffraction limit, the lens objective needs to be positioned via a motion stage with a resolution of less than 100 nm to measure the beam waist in a controlled way by moving the spot in the focus.

Ac Stark Shift and Beam Waist. After the ODT is established, the ion is irradiated by the high-power dipole laser in the trap center. The interaction between the ion and the laser beam leads to an intensity-dependent shift, known as the ac Stark shift, of its electronic energy levels. This shift causes an obvious shift of the fluorescence spectrum of the $^{40}Ca^{+}$ ion's dipole transition $4S_{1/2} \leftrightarrow 4P_{1/2}$.

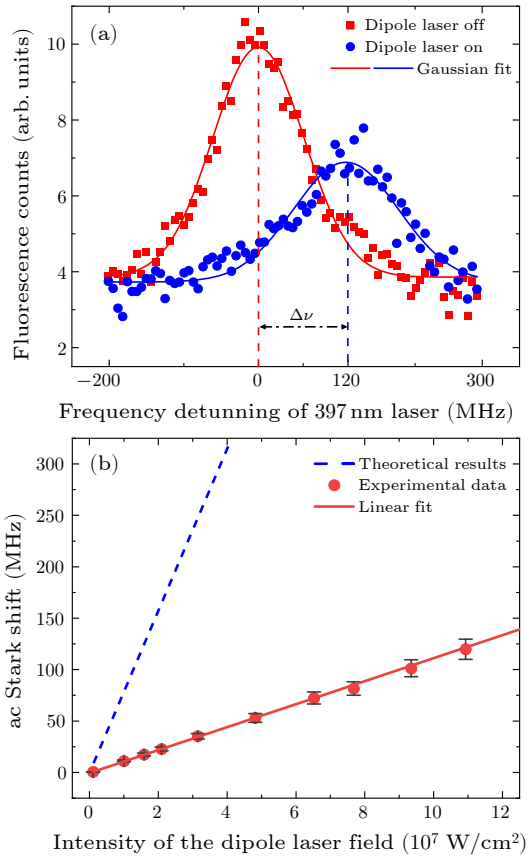

Fig. 3. (a) The fluorescence spectrum of the $^{40}Ca^{+}$ ion's dipole transition $4S_{1/2} \leftrightarrow 4P_{1/2}$. (b) Experimental measurements and theoretical calculations of ac Stark shifts under different dipole laser intensities.

As depicted in Fig. 3(a), we scanned the frequency detuning (the horizontal axis) of the dipole transition laser at 397 nm with the dipole laser both on and off to obtain the ion's fluorescence spectra under these two conditions. It can be observed that the presence of the dipole laser induces a frequency shift ($\Delta\nu$) in the fluorescence spectrum, which is corresponding to the ac Stark shift. In Fig. 3(b), the red solid line represents the experimental measured ac Stark shift, which is proportional to the power density of the dipole trap laser, and the highest power density of the dipole laser results in the maximum ac Stark shift of $\sim 120\,\text{MHz}$. The dashed line in Fig. 3(b) indicates the theoretical upper bound for this measurement, which will be discussed in the following.

Also shown in Fig. 3(a), the ac Stark shift results in a significant reduction in fluorescence counts at the resonance frequency of the dipole transition (where the detuning is 0). The fluorescence counts noticeably decrease from the red line to the blue line. When the dipole laser power density is fixed, the degree of fluorescence count attenuation at resonance is positively correlated with the overlap between the dipole laser and the ion. In other words, for ions positioned at the center of the trap, the spatial distribution of fluorescence observed by scanning the dipole trap position exhibits an inverse relationship with laser intensity. This allows for controlled measurement of the beam waist by adjusting the focal spot: fluorescence counts at the resonance frequency of the dipole transition laser (397 nm) diminish most significantly when the ion's position is perfectly aligned with the dipole laser's focal spot.

With a 10 nm resolution piezoelectric transducer (PZT) displacement stage (Physik Instrumente, P-611XZ), we scanned the radial two-dimensional coordinates (x- and y-axes in Fig. 4) of the spot in focus to obtain the spatial distribution of dipole laser intensity. By fitting the data with a Gaussian function, we obtained the beam waist radii in the x- and y-axes are $w_x = 2.12(9)\,\mu\text{m}$ and $w_y = 1.33(9)\,\mu\text{m}$, respectively. These results enable us to determine the $1/e^2$ intensity waist radius of the dipole light as $w_0 = \sqrt{(w_x^2 + w_y^2)/2} \approx 1.77(13)\,\mu\text{m}$, which is near the diffraction limit w_{min} and is only half of the result in our previous work.[34]

Dipole Potential and Ion Temperature. For a far-detuned dipole laser with frequency ω, the dipole potential U_{dip} of the ODT reads[33]

$$U_{\text{dip}}(\boldsymbol{r}) = -\frac{3\pi c^2}{2\omega_0^3}\left(\frac{\Gamma}{\omega_0 - \omega} + \frac{\Gamma}{\omega_0 + \omega}\right) I(\boldsymbol{r}), \tag{2}$$

where c is the speed of light in vacuum. For a $^{40}Ca^{+}$ ion, $\omega_0 = 2\pi c/(397\,\text{nm})$ and $\Gamma \approx 2\pi \times 22\,\text{MHz}$ represent the frequency and the natural linewidth of the dipole resonant transition ($4S_{1/2} \leftrightarrow 4P_{1/2}$, as shown in Fig. 2), respectively. Moreover, the intensity of the dipole laser field $I(\boldsymbol{r})$ is given as

$$I(\boldsymbol{r}) = \frac{2P}{\pi w^2(z)} \exp\left(-\frac{2r^2}{w^2(z)}\right), \tag{3}$$

where P is the laser power, r and z represent the coordinates in the cylindrical coordinate system in Fig. 1, and $w(z)$ denotes the spot size parameter. By utilizing the experimental parameters and these equations, we determined the peak laser intensity of the ODT: $I_{\text{max}} = I(r = 0, z = 0) = \frac{2P_{\text{enter}}}{\pi w_0^2} \approx 1.09 \times 10^8\,\text{W}\cdot\text{cm}^{-2}$, and calculated the dipole potential to be $U_{\text{max}} \approx -h \times 860\,\text{MHz}$, where h is Planck's constant, serving as the theoretical upper bound. However, the actual dipole potential is significantly lower

than the upper bound, primarily due to the non-Gaussian profile of the dipole laser and the aberration and diffraction effects cause by the entrenched vacuum viewport on the dipole laser. In addition, the ion's thermal motion caused by the laser heating induced by dipole laser contributed largely to the mismatch.

In this work, we evaluated the actual dipole potential by measuring the ac Stark shift caused by the dipole laser, as the ac Stark shift of the ground state $4S_{1/2}$ energy level equals the dipole potential in value with the approximation of an oscillator model.[33] The measured ac Stark shift reaches a maximum of $|U_{\rm dip}(S_{1/2})//h| \approx 120\,{\rm MHz}$, at the maximal power of $P_{\rm enter} = 5.38\,{\rm W}$ in Fig. 4. Thus, the corresponding potential depth of the ODT amounts to $U_{\rm dip} \approx -k_{\rm B} \times 5.76$ mK, where $k_{\rm B}$ is Boltzmann's constant.

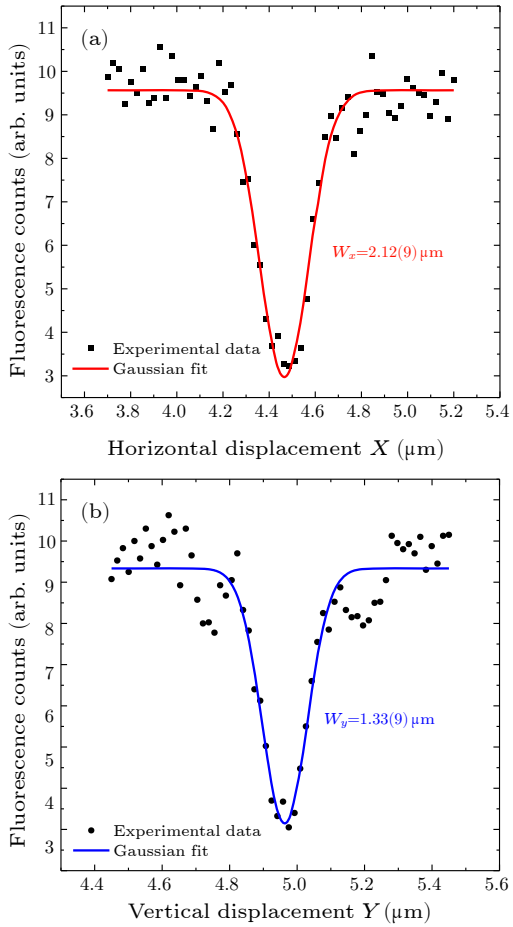

Fig. 4. (a) Data (square dots) obtained by scanning the displacement stage along the x-axis and the corresponding fitting results (red line). (b) Data (round dots) obtained by scanning the displacement stage along the y-axis and the corresponding fitting results (blue line).

As mentioned earlier, one of the prerequisites for optical trapping is that the trapping potential of the ODT should be higher than the kinetic energy of the ion. To obtain the ion's kinetic energy, it is necessary to measure the temperature of the $^{40}Ca^{+}$ ion. In this work, we employed a method that relies on the temperature-dependent spread of the time-averaged position of the ion for temperature measurement.[35] The relationship between the ion's spatial distribution and their trapping potential (secular frequency, ω) is associated with their temperature T:[35]

$$w_{\rm CCD} = \sqrt{w_{\rm PSF}^2 + \frac{k_{\rm B}T}{m\omega^2}}, \tag{4}$$

where m represents the ion mass, $w_{\rm CCD}$ is the imaging linewidth of ions on the CCD camera (Gaussian fitting), and $w_{\rm PSF}$ is the RMS resolution of the imaging system's point spread function (PSF), which is a constant value for a specific imaging system. In our experiment, the detection direction of the CCD camera is along the x-axis, making it easy to observe the manifestation of the axial secular motion frequency ω_z on the ion imaging. By measuring the spot sizes $w_{\rm CCD}$ for different ω_z and fitting them with Eq. (4), as shown in Fig. 5, we accurately determined the temperature of the $^{40}Ca^{+}$ ion after Doppler cooling to be $T_{\rm ion} = 0.93(3)\,{\rm mK}$. Kinetic energy of the $^{40}Ca^{+}$ ion $E_{\rm k} = k_{\rm B} \times T_{\rm ion}$ is lower than the dipole potential value $|U_{\rm dip}|$, ensuring the prerequisite of optical trapping.

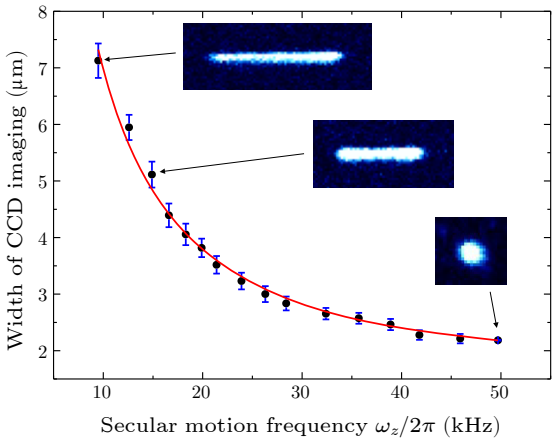

Fig. 5. Measurement of the spot size of the ion images after Doppler cooling for various trapping potential, $\omega_z/2\pi$. The insets are exemplary ion images.

Dipole Force and Residual Force. Similar to Eq. (2), for a far-detuned dipole laser, the corresponding dipole force $F_{\rm dip}$ is[33]

$$F_{\rm dip}(\boldsymbol{r}) = -\nabla U_{\rm dip}(\boldsymbol{r}) = \frac{3\pi c^2}{2\omega_0^3}\Big(\frac{\Gamma}{\omega_0-\omega} + \frac{\Gamma}{\omega_0+\omega}\Big)\nabla I(\boldsymbol{r}), \tag{5}$$

where ∇ denotes the Nabla operator (gradient operator). Then, the maximum radial dipole force can be calculated by

$$(F_{{\rm dip},\,r})_{\rm max} = \frac{3\pi c^2}{2\omega_0^3}\Big(\frac{\Gamma}{\omega_0-\omega} + \frac{\Gamma}{\omega_0+\omega}\Big)\Big(\frac{\partial I}{\partial r}\Big)_{r=w_0/2} \approx -4\times10^{-19}\,{\rm N}. \tag{6}$$

To ensure another prerequisite of optical trapping, the residual force of stray electric fields at the ion's position should be at least a level smaller than the maximal dipole force of the ODT, which necessitates the precise compensation for stray electric fields.

In this work, we utilize the ion's position in fluorescence imaging on the CCD camera (shown as the inset in Fig. 5) as an indicator to precisely compensate for stray electric fields.[36] This method is based on measuring the displacement of a trapped ion induced by an electric field. In this experiment, we employed another CCD camera detecting along the z-axis direction to observe ions, and the radial secular motion frequency was initially set as $\omega_{r,\,\mathrm{h}} \approx 2\pi \times 888\,\mathrm{kHz}$. Meanwhile, our imaging system, as shown in Fig. 6(a), is capable of achieving ion observation with a spatial resolution of up to 2 μm.

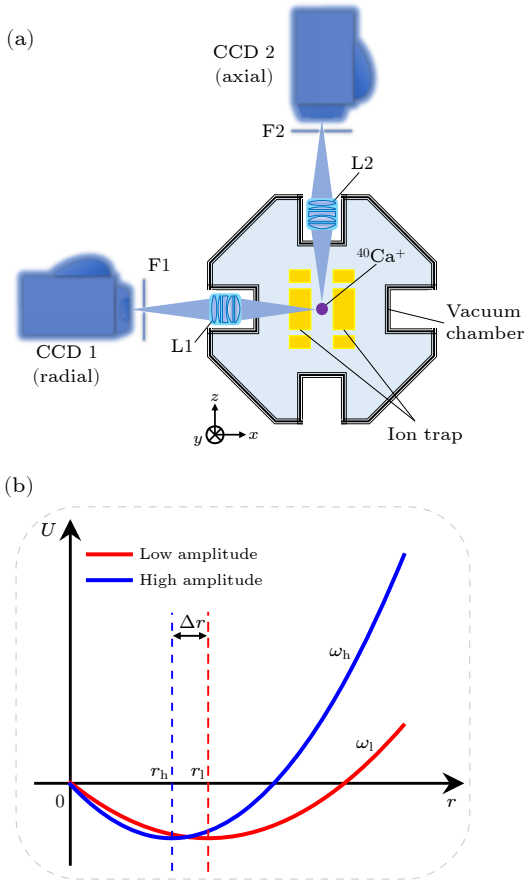

Fig. 6. (a) Schematic diagram of the imaging system. CCD: charge-coupled-device camera; F: filter; L: imaging lens. (b) Illustration of the trapping harmonic potential of different RF amplitudes.

For an ion with mass m trapped in Paul traps with a radial secular motion frequency of ω_r, the potential of RF fields can be expressed as a harmonic potential field:

$$U(r) = \frac{m\omega_r^2 r^2}{2}, \tag{7}$$

where r represents the radial distance of the ion from its equilibrium position. Taking into account the influence of the stray electric field $\varepsilon(r)$, the potential field in which the ^{40}Ca$^+$ ion is located can be expressed as

$$U(r) = \frac{m\omega_r^2 r^2}{2} - q\varepsilon(r)r, \tag{8}$$

where q denotes the charge of the ion. From this, it can be inferred that the stable position of the ion is the location where the potential field is at its minimum, i.e.,

$$r = \frac{q\varepsilon(r)}{m\omega_r^2}. \tag{9}$$

The inset in Fig. 6(b) illustrates a schematic diagram of the trapping harmonic potential field under different RF amplitudes. By measuring the changes in ion position as the RF amplitude is varied between high and low values, conclusions can be drawn in regard of

$$\Delta r = r_\mathrm{l} - r_\mathrm{h} = \frac{q\varepsilon(r)}{m\omega_{r,\mathrm{l}}^2} - \frac{q\varepsilon(r)}{m\omega_{r,\mathrm{h}}^2}. \tag{10}$$

Thus, the stray electric field can be derived as follows:

$$\varepsilon(r) = \frac{m\omega_{r,\mathrm{h}}^2\omega_{r,\mathrm{l}}^2\Delta r}{q(\omega_{r,\,\mathrm{h}}^2 - \omega_{r,\,\mathrm{l}}^2)}. \tag{11}$$

During the compensation for stray electric fields, we set the low RF amplitude at 12.5% of the initial amplitude, corresponding to a secular motion frequency $\omega_{r,\,\mathrm{l}} \approx 2\pi \times 111\,\mathrm{kHz}$. As the displacement of a ^{40}Ca$^+$ ion reaches 2 μm, limited by the resolution of the imaging system in our experiment, the corresponding stray electric field is $|\varepsilon_r|10\,\mathrm{mV/m}$ according to Eq. (11) after the compensation. Subsequently, the residual force of the stray electric field is $F_\mathrm{stray} \leq 1.6 \times 10^{-21}\,\mathrm{N}$ at the ion's position, and is two levels smaller than the maximal dipole force $F_{\mathrm{dip},\,r}$ of the ODT, ensuring the prerequisite for optical trapping.

Additionally, the stray electric field throughout the process is not static but has an inherent drift over the entire experiment, primarily caused by the decay over time of free charges attached to dielectrics such as the entrenched viewports of the vacuum chamber. This makes the compensation for stray electric fields not a one-time occurrence but a continuous process throughout the experiment. To suppress the drift of stray electric fields, we implemented two effective measures in this work: (1) We used the pulse-laser-ablation (PLA) method[37] instead of the traditional photo-ionization method[38] for loading ^{40}Ca$^+$ ions to minimize the generation of free charges. Additionally, the PLA method can effectively prevent the deposition of calcium on the trap electrodes and precisely load the single ^{40}Ca$^+$ ion for optical trapping. (2) We coated the entrenched viewports of the vacuum chamber with indium-tin-oxide (ITO) glasses,[39] which can prevent the accumulation of free charges on the viewports due to their conductivity. After these adjustments, we can extend the compensation period for stray electric fields to once a day, effectively enhancing the overall effective time of the experiment.

Experimental Procedure. The entire time sequence for the optical trapping experiment is illustrated in Fig. 7. Initially, we perform pre-cooling and Doppler cooling of the ion for 2000 μs and 1000 μs, respectively, where the height of the colored blocks represents the laser power. Subsequently, we deactivate the RF field once the dipole potential trap is confirmed to be established by the dipole laser and maintain the ODT for a delay time Δt_opt. Following this, the RF field is reactivated while the ODT is deactivated, and the fluorescence light scattered off the ion is monitored again through the CCD camera to determine if

the ion was lost after the experimental sequence. If the ion is still present, indicating successful optical trapping, we repeat the sequence until the ion is lost. By repeating the experiment multiple times, we can compile the total number of experimental sequences, $N_{\rm tot}$, and the number of successful trapping attempts for each parameter set, $N_{\rm opt}$. The probability of optically trapping $^{40}Ca^{+}$ ions, $p_{\rm opt}$, calculated as $p_{\rm opt} = N_{\rm opt}/N_{\rm tot}$ for the dipole trap duration $\Delta t_{\rm opt}$. The asymmetric uncertainties of this probability are determined by the maximum value of the underlying binomial probability density function and the corresponding 1σ-Wilson-score interval.[40]

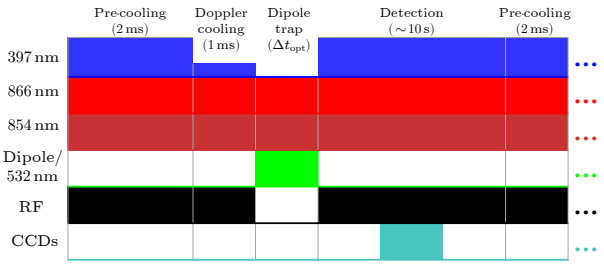

Fig. 7. The time sequence for optical trapping (not to scale).

To improve the probability of optical trapping for longer durations, we incorporated two measures throughout the entire experimental procedure:

(1) Mitigating electron shelving of the dipole laser in metastable states. Specifically, for $^{40}Ca^{+}$ ions, the dipole laser (532 nm) serves as a blue-detuned laser for the $D \leftrightarrow P$ transition, resulting in repulsive potential optical traps as $U_{\rm dipole}(D_{3/2})$ and $U_{\rm dipole}(D_{5/2})$. This repulsion leads to a loss of the $^{40}Ca^{+}$ ion, decreasing the trapping probability for trapping duration, which is called the electron shelving of the dipole laser in metastable states. To mitigate the electron shelving mechanism, we employed repumping light (866 nm) and quenching light (854 nm), both with beam waist radii of approximately 100 μm and saturated power levels, to depopulate the D manifolds in the dipole trapping duration $\Delta t_{\rm opt}$.

(2) Ramping down the RF voltage within a careful choice of period. We need to minimize the impact of the inevitable violation of the stability criteria of the RF field during the shutdown and establishment period. In our work, deactivating the RF field during experimental operation is accomplished by switching the RF output port through a switching circuit (Mini-circuits, ZASW-2-50DRA+). Voltage changes during the process of turning off the RF for a specific period ($\Delta t_{\rm opt} = 500$ μs) and then turning it back on were measured using an antenna placed near the helical resonator, as depicted in Fig. 8. Experimental data indicate that the relaxation time for RF field deactivation is approximately 20 μs, effectively preventing additional heating from higher-order resonances.[41] This approach also minimizes the heating effect on ions resulting from non-adiabatic transport. On the other hand, the establishment of the dipole potential field is regulated by a custom made with a response delay of around 1 μs. The measured rising/falling edge time of the dipole laser is within 500 ns, and these two time delays are subtracted from the experimental timing sequence.

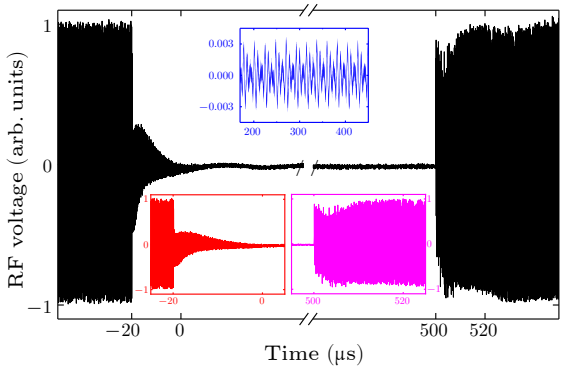

Fig. 8. RF voltage of the RF trap during the experimental sequence. The three color-coded insets show magnified details of RF ramping down, closed, and restarting, respectively.

Experimental Results. To determine the optical trapping lifetime of the $^{40}Ca^{+}$ ion in the ODT, we measured the optical trapping probability $p_{\rm opt}$ as a function of the dipole trap duration $\Delta t_{\rm opt}$, as shown in Fig. 9. Each data point is an average of approximately 60 experimental sequences, with error bars representing the 1σ confidence interval.

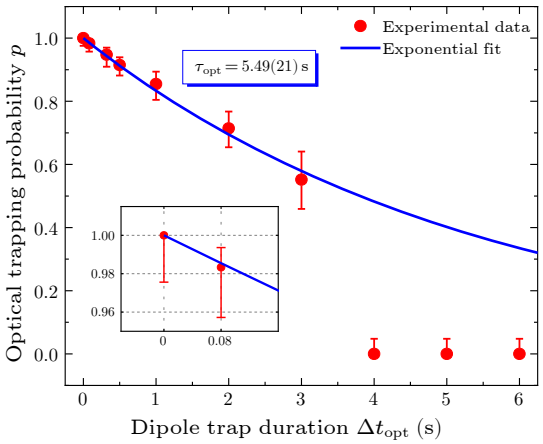

Fig. 9. Measurement results of the lifetime of optical trapping for a $^{40}Ca^{+}$ ion.

Notably, the probability of optically trapping has exceeded 98% for the dipole trap duration $\Delta t_{\rm opt} = 80$ ms, which is the level of interrogation time for the clock transition of $^{40}Ca^{+}$ ion clocks.[16,17] The optical trapping probability reaches 0 for dipole trap durations over 3 s, indicating that no successful attempts are recorded for these dipole trap durations. The main reason of ion loss for dipole trap durations over 3 s is "ion temperature" which means the heating effect caused by photon recoils out of the ODT.[23] However, for the sudden drop of trapping probability exceed 3 s, we have not clearly identified the cause of this phenomenon, and one plausible explanation is the presence of electromagnetic disturbances with a periodicity near 3 s in the experimental environment, such as

oscillations in the voltage source supplying the dc trapping field or power line interference from various equipment in the laboratory. Nevertheless, by fitting the results with a simplified exponential model (as represented by the solid line in Fig. 9), the optical trapping lifetime of the $^{40}Ca^{+}$ ion under these conditions, corresponding to the trapping duration at $1/e$ trapping probability, is determined to be $\tau_{\rm opt} > 3\,{\rm s}$. Such long lifetimes make it possible to apply the optical trapping technique to different fields of ion research.

In summary, utilizing our newly developed all-optical trapping experimental platform, we have successfully achieved the first optical trapping of a $^{40}Ca^{+}$ ion without any RF fields. By employing techniques such as focusing the dipole beam waist near the diffraction limit, precisely compensating for stray electric fields, and mitigating electron shelving in metastable states, we demonstrated the longest optical trapping lifetime of over 3 s for a single $^{40}Ca^{+}$ ion. Notably, we have consistently achieved an optical trapping possibility success rate 98% for trapping time of approximately 100 ms (specifically 80 ms), which is crucial for $^{40}Ca^{+}$ ion optical clocks. This work could pave the way for development of all-optical trapping ion optical clocks.

Furthermore, the dipole laser used for $^{40}Ca^{+}$ ion's all-optical trapping can be chosen at a magic wavelength, which means that the ac Stark shifts caused by the dipole laser will be zero.[42–45] Thus, the optical trapping potential will introduce no shift in the clock transition frequency. Therefore, for a magic-wavelength optically trapped $^{40}Ca^{+}$ ion, both micromotion and ac Stark shift of the clock transition can be greatly suppressed, which will improve the accuracy of the $^{40}Ca^{+}$ ion optical clock. In addition to the accuracy of an optical clock, the frequency stability is also an important issue when evaluating an optical clock. Compared to neutral-atom lattice clocks,[3,46–48] the stability of a single ion clock is limited by the quantum projection noise limit[49] because the ion number N is only one. Recently, the optical trapping of Coulomb ion crystals has been demonstrated by Schaetz's group.[27,50] Thus, the optical trapping technique for ions will shed light on development of all-optical trapping ion clocks using multiple ions to achieve better frequency stability.

Acknowledgements. This work was supported by the National Basic Research R&D Program of China (Grant Nos. 2022YFB3904001 and 2018YFA0307500), the National Natural Science Foundation of China (Grant Nos. 12022414 and 11934014), the Natural Science Foundation of Hubei Province (Grant No. 2022CFA013), and the CAS Project for Young Scientists in Basic Research (Grant Nos. YSBR-085 and YSBR-055).

We thank Yanmei Hao for the help of laser techniques; Shanshan Lu, Fangfei Wu, Liyan Tang and Chengbin Li for their assistance in theoretical calculations; Sebastian Knuenz for the support with temperature measurements; Jun Jiang for the assistance in revising the paper; and Hu Shao, Wanli Yang for their fruitful discussions. We are also grateful to Tobias Schaetz, Christian Schneider, Julian Schmidt, Leon Karpa and Wei Wu for their helpful discussions and suggestions.

References

[1] Brewer S M, Chen J S, Hankin A M, Clements E R, Chou C W, Wineland D J, Hume D B and Leibrandt D R 2019 *Phys. Rev. Lett.* **123** 033201
[2] Zhiqiang Z, Arnold K J, Kaewuam R, and Barrett M D 2023 *Sci. Adv.* **9** eadg1971
[3] Aeppli A, Kim K, Warfield W, Safronova M S, and Ye J 2024 *Phys. Rev. Lett.* **133** 023401
[4] Cai Z, Luan C Y, Ou L, Tu H, Yin Z, Zhang J N, and Kim K 2023 *J. Korean Phys. Soc.* **82** 882
[5] Evered S J, Bluvstein D, Kalinowski M, Ebadi S, Manovitz T, Zhou H, Li S H, Geim A A, Wang T T, Maskara N, Levine H, Semeghini G, Greiner M, Vuletić V, and Lukin M D 2023 *Nature* **622** 268
[6] Paul W 1990 *Rev. Mod. Phys.* **62** 531
[7] Phillips W D 1998 *Rev. Mod. Phys.* **70** 721
[8] Kiesenhofer D, Hainzer H, Zhdanov A, Holz P C, Bock M, Ollikainen T, and Roos C F 2023 *PRX Quantum* **4** 020317
[9] Bloch D, Hofer B, Cohen S R, Browaeys A, and Ferrier-Barbut I 2023 *Phys. Rev. Lett.* **131** 203401
[10] Schäfer F, Fukuhara T, Sugawa S, Takasu Y, and Takahashi Y 2020 *Nat. Rev. Phys.* **2** 411
[11] Cetina M, Grier A T, and Vuletić V 2012 *Phys. Rev. Lett.* **109** 253201
[12] Nguyên L H, Kalev A, Barrett M D, and Englert B G 2012 *Phys. Rev. A* **85** 052718
[13] Ushijima I, Takamoto M, Das M, Ohkubo T, and Katori H 2015 *Nat. Photon.* **9** 185
[14] Huntemann N, Sanner C, Lipphardt B, Tamm Chr, and Peik E 2016 *Phys. Rev. Lett.* **116** 063001
[15] McGrew W F, Zhang X, Fasano R J, Schäffer S A, Beloy K, Nicolodi D, Brown R C, Hinkley N, Milani G, Schioppo M, Yoon T H, and Ludlow A D 2018 *Nature* **564** 87
[16] Huang Y, Zhang B, Zeng M, Hao Y, Ma Z, Zhang H, Guan H, Chen Z, Wang M, and Gao K 2022 *Phys. Rev. Appl.* **17** 034041
[17] Zeng M, Huang Y, Zhang B, Hao Y, Ma Z, Hu R, Zhang H, Chen Z, Wang M, Guan H, and Gao K 2023 *Phys. Rev. Appl.* **19** 064004
[18] Huang Y, Guan H, Liu P, Bian W, Ma L, Liang K, Li T, and Gao K 2016 *Phys. Rev. Lett.* **116** 013001
[19] Tomza M, Jachymski K, Gerritsma R, Negretti A, Calarco T, Idziaszek Z, and Julienne P S 2019 *Rev. Mod. Phys.* **91** 035001
[20] Härter A and Hecker Denschlag J 2014 *Contemp. Phys.* **55** 33
[21] Pagano G, Hess P W, Kaplan H B, Tan W L, Richerme P, Becker P, Kyprianidis A, Zhang J, Birckelbaw E, Hernandez M R, Wu Y, and Monroe C 2018 *Quantum Sci. Technol.* **4** 014004
[22] Yum D and Choi T 2022 *Curr. Appl. Phys.* **41** 163
[23] Schneider Ch, Enderlein M, Huber T, and Schaetz T 2010 *Nat. Photon.* **4** 772
[24] Huber T, Lambrecht A, Schmidt J, Karpa L, and Schaetz T 2014 *Nat. Commun.* **5** 5587
[25] Lambrecht A, Schmidt J, Weckesser P, Debatin M, Karpa L, and Schaetz T 2017 *Nat. Photon.* **11** 704
[26] Enderlein M, Huber T, Schneider C, and Schaetz T 2012 *Phys. Rev. Lett.* **109** 233004
[27] Schmidt J, Lambrecht A, Weckesser P, Debatin M, Karpa L, and Schaetz T 2018 *Phys. Rev. X* **8** 021028
[28] Schmidt J, Weckesser P, Thielemann F, Schaetz T, and Karpa L 2020 *Phys. Rev. Lett.* **124** 053402
[29] Weckesser P, Thielemann F, Wiater D, Wojciechowska A, Karpa L, Jachymski K, Tomza M, Walker T, and Schaetz T 2021 *Nature* **600** 429
[30] Dubé P, Madej A A, Zhou Z, and Bernard J E 2013 *Phys. Rev. A* **87** 023806

[31] Godun R M, Nisbet-Jones P B R, Jones J M, King S A, Johnson L A M, Margolis H S, Szymaniec K, Lea S N, Bongs K, and Gill P 2014 *Phys. Rev. Lett.* **113** 210801

[32] Oskay W H, Diddams S A, Donley E A, Fortier T M, Heavner T P, Hollberg L, Itano W M, Jefferts S R, Delaney M J, Kim K, Levi F, Parker T E, and Bergquist J C 2006 *Phys. Rev. Lett.* **97** 020801

[33] Grimm R, Weidemüller M and Ovchinnikov Y B 2000 *Advances in Atomic, Molecular, and Optical Physics* (Amsterdam: Elsevier) vol 42 p 95

[34] Wang M, Chen Z, Huang Y, Guan H, and Gao K L 2021 *Chin. Phys. B* **30** 053702

[35] Knünz S, Herrmann M, Batteiger V, Saathoff G, Hänsch T W, and Udem Th 2012 *Phys. Rev. A* **85** 023427

[36] Berkeland D J, Miller J D, Bergquist J C, Itano W M, and Wineland D J 1998 *J. Appl. Phys.* **83** 5025

[37] Shao H, Wang M, Zeng M, Guan H, and Gao K 2018 *J. Phys. Commun.* **2** 095019

[38] Gulde S, Rotter D, Barton P, Schmidt-Kaler F, Blatt R, and Hogervorst W 2001 *Appl. Phys. B* **73** 861

[39] Wang M, Chen Z, Huang Y, Guan H, and Gao K L 2023 *Chin. J. Quantum Electron.* **40** 127

[40] Wilson E B 1927 *J. Am. Stat. Assoc.* **22** 209

[41] Drakoudis A, Söllner M, and Werth G 2006 *Int. J. Mass Spectrom.* **252** 61

[42] Liu P L, Huang Y, Bian W, Shao H, Guan H, Tang Y B, Li C B, Mitroy J, and Gao K L 2015 *Phys. Rev. Lett.* **114** 223001

[43] Huang Y, Wang M, Chen Z, Li C, Zhang H, Zhang B, Tang L, Shi T, Guan H, and Gao K L 2024 *New J. Phys.* **26** 043021

[44] Jiang J, Jiang L, Wu Z W, Zhang D H, Xie L Y, and Dong C Z 2019 *Phys. Rev. A* **99** 032510

[45] Jiang J, Jiang L, Wang X, Zhang D H, Xie L Y, and Dong C Z 2017 *Phys. Rev. A* **96** 042503

[46] Dimarcq N, Gertsvolf M, Mileti G, Bize S, Oates C W, Peik E, Calonico D, Ido T, Tavella P, Meynadier F, Petit G, Panfilo G, Bartholomew J, Defraigne P, Donley E A, Hedekvist P O, Sesia I, Wouters M, Dubé P, Fang F, Levi F, Lodewyck J, Margolis H S, Newell D, Slyusarev S, Weyers S, Uzan J P, Yasuda M, Yu D H, Rieck C, Schnatz H, Hanado Y, Fujieda M, Pottie P E, Hanssen J, Malimon A, and Ashby N 2024 *Metrologia* **61** 012001

[47] Kim H, Heo M S, Park C Y, Yu D H, and Lee W K 2021 *Metrologia* **58** 055007

[48] Zhang A, Xiong Z, Chen X, Jiang Y, Wang J, Tian C, Zhu Q, Wang B, Xiong D, He L, Ma L, and Lyu B 2022 *Metrologia* **59** 065009

[49] Dubé P, Madej A A, Shiner A, and Jian B 2015 *Phys. Rev. A* **92** 042119

[50] Hoenig D, Thielemann F, Karpa L, Walker T, Mohammadi A, and Schaetz T 2024 *Phys. Rev. Lett.* **132** 133003